Cell Reports

Article

Acetylation of UHRF1 Regulates Hemi-methylated DNA Binding and Maintenance of Genome-wide DNA Methylation

Graphical Abstract

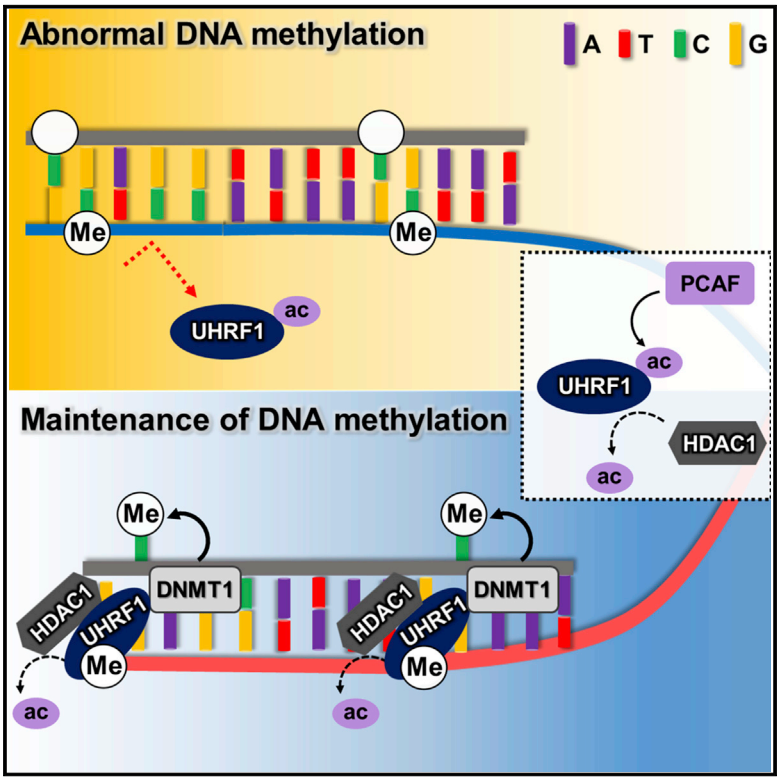

Highlights

- Acetylation of UHRF1 is regulated by PCAF and HDAC1
- PCAF-mediated UHRF1 acetylation disrupts its hemi-methylated DNA binding
- Deacetylation by HDAC1 is required for chromatin association of UHRF1 during S phase
- Deregulation of UHRF1 acetylation impedes the inheritance of global DNA methylation

Authors

Ja Young Hahm, Jin Woo Park, Joo-Young Kang, ..., Nam-Chul Ha, Jung-Woong Kim, Sang-Beom Seo

Correspondence

sangbs@cau.ac.kr

In Brief

Hahm et al. describe a regulatory mechanism of UHRF1 in DNA methylation maintenance. UHRF1 acetylation by PCAF at lysine 490 disrupts the binding affinity of UHRF1 to hemi-methylated DNA in nascent DNA. These findings suggest that fine-tuned acetylation of UHRF1 is essential for inheritance of epigenomic information.

Hahm et al., 2020, Cell Reports *32*, 107958
July 28, 2020
https://doi.org/10.1016/j.celrep.2020.107958

CellPress

Cell Reports

CellPress
OPEN ACCESS

Article

Acetylation of UHRF1 Regulates Hemi-methylated DNA Binding and Maintenance of Genome-wide DNA Methylation

Ja Young Hahm,[1] Jin Woo Park,[1] Joo-Young Kang,[1] Junyoung Park,[1] Chul-Hong Kim,[1] Ji-Young Kim,[1] Nam-Chul Ha,[2] Jung-Woong Kim,[1] and Sang-Beom Seo[1,3,*]

[1]Department of Life Science, College of Natural Sciences, Chung-Ang University, Seoul 06974, Republic of Korea
[2]Department of Agricultural Biotechnology, Seoul National University, Seoul 08826, Republic of Korea
[3]Lead Contact
*Correspondence: sangbs@cau.ac.kr
https://doi.org/10.1016/j.celrep.2020.107958

SUMMARY

UHRF1 is a key regulator in DNA methylation maintenance. It binds histone H3K9me2/3 and hemi-methylated DNA and recruits DNMT1 to DNA replication forks during S phase. However, the regulatory mechanism of hemi-methylated DNA binding activity of UHRF1 remains unknown. In this study, we reveal that acetylation of UHRF1 is regulated by PCAF and HDAC1. We show that UHRF1 acetylation at K490 attenuates its binding affinity to hemi-methylated DNA. We analyze genome-wide DNA methylation and gene-expression patterns using stable cell lines and discover that cells where the endogenous UHRF1 is replaced with an acetyl-mimetic (UHRF1 K490Q) mutant show deficiencies in inherited DNA methylation and show different gene-expression patterns in genes related to cell survival. These results reveal that precise regulation of UHRF1 acetylation is required to maintain DNA methylation during cell division and control cell survival.

INTRODUCTION

As the most-studied mechanism of epigenetic regulation, DNA methylation is essential in the maintenance of cellular identities (Kulis and Esteller, 2010). During cell division, inheritance of DNA methylation patterns is tightly regulated by the DNA methylation maintenance machinery, including ubiquitin-like with PHD and RING finger domains 1 (UHRF1) (Chuang et al., 1997).

UHRF1 is integral in the maintenance of DNA methylation as it recruits DNMT1 to DNA replication foci. Knockout (KO) of UHRF1 in mouse embryonic stem cell resulted in a global loss of DNA methylation and a lethal phenotype (Bostick et al., 2007; Sharif et al., 2007). UHRF1 recognizes and binds to newly synthesized hemi-methylated DNA at replication forks through its unique SRA (SET and RING-associated) domain. Specifically, the NKR finger (483–496 residues) in the SRA domain is the key sub-motif that recognizes hemi-methylated DNA and directs DNMT1 to newly synthesized DNA (Arita et al., 2008; Avvakumov et al., 2008; Frauer et al., 2011; Hashimoto et al., 2008). Recent studies have shown that SRA domain mutants, which abrogate hemi-methylated DNA binding, are incapable of maintaining genomic DNA methylation patterns (Kong et al., 2019; Liu et al., 2013).

Here, we found that acetylation of UHRF1 is tightly regulated by P300/CBP-associated factor (PCAF) and histone deacetylase 1 (HDAC1) at residue K490. We determined that acetylation of UHRF1 impedes hemi-methylated DNA binding both *in vivo* and *in vitro*. Finally, we analyzed UHRF1 acetylation-dependent DNA methylation and gene-expression patterns at global level and showed that acetyl-mimetic substitution of UHRF1 at K490 resulted in a failure to maintain genome-wide DNA methylation and changes gene-expression patterns.

RESULTS

UHRF1 Is Acetylated at K490 by PCAF

It has been known that hemi-methylated DNA binding by UHRF1 is mainly responsible for the maintenance of DNA methylation in daughter cells. However, the regulatory mechanism of UHRF1 during epigenetic inheritance is still unclear. In this study, we set out to focus on uncovering the posttranslational modification responsible for facilitating UHRF1 hemi-methylated DNA binding. Immunoprecipitation (IP) assays were performed using an anti-pan-acetyl-lysine or anti-UHRF1 antibody, and these analyses revealed that UHRF1 could be acetylated in HCT116 cells (Figure 1A). To identify which acetyltransferase catalyzes this reaction, we performed *in vitro* acetylation assays using different histone acetyltransferases, p300, PCAF, and CBP. Of these, PCAF showed the strongest catalytic activity toward acetylation of UHRF1 (data not shown). In addition, the acetylation of UHRF1 was enhanced by increasing the amount of available PCAF (Figure 1B). To identify which lysine residues were responsible for this acetylation, we mapped the domains of UHRF1 acetylated by PCAF. *In vitro* acetylation assays were performed using fragments of UHRF1 and found that PCAF acetylates UHRF1 within the SRA domain (Figure 1C). The reciprocal coIP assays

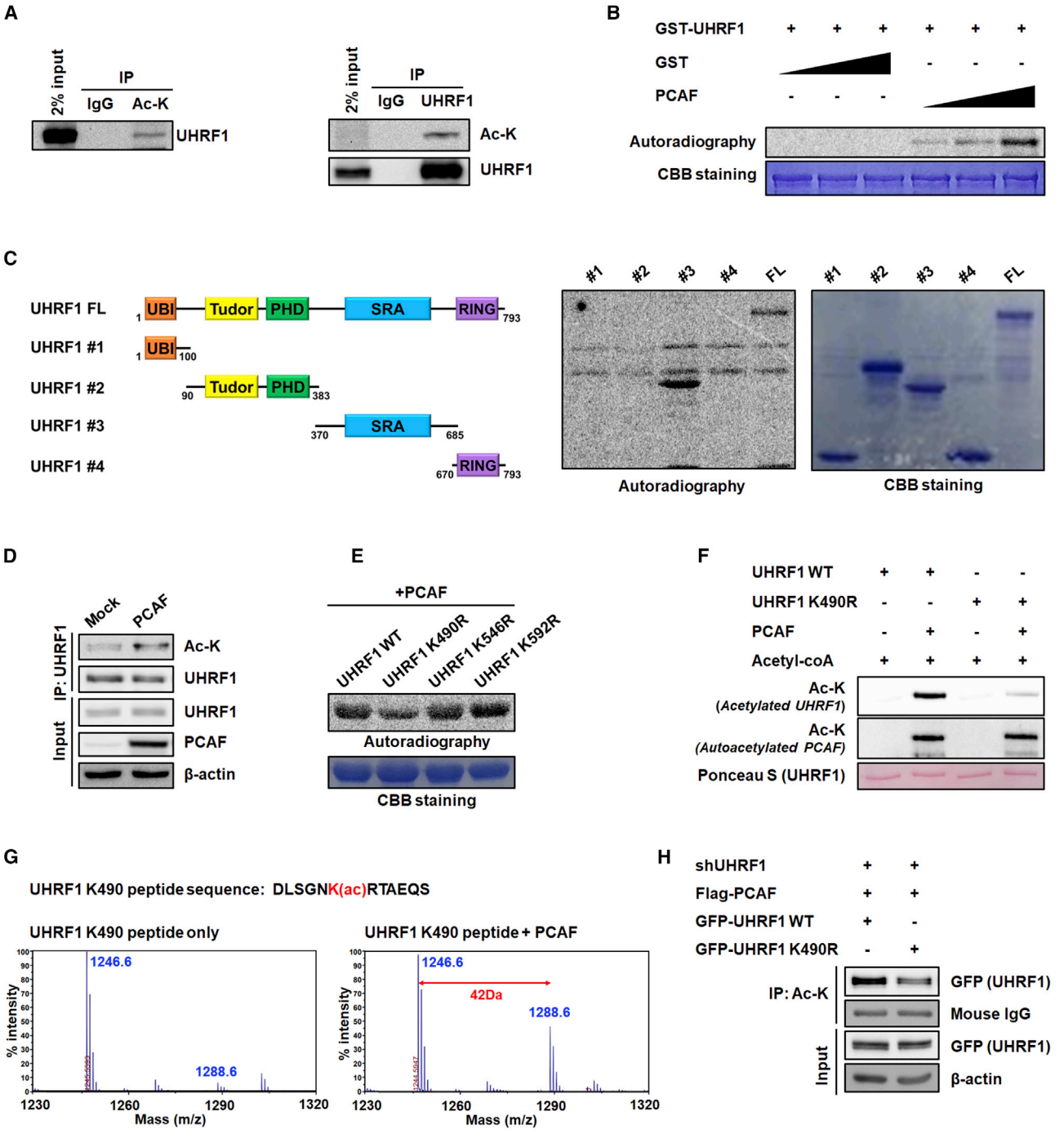

Figure 1. UHRF1 Is Acetylated at K490 by PCAF *In Vivo* and *In Vitro*

(A) HCT116 cells were immunoprecipitated using control immunoglobulin G (IgG), anti-UHRF1, or anti-acetyl-lysine antibodies and evaluated by western blots.

(B) Full-length GST-fusion UHRF1 was incubated with [^{14}C]-acetyl-CoA and PCAF for 3 h at 30°C, separated by SDS-PAGE, and visualized using autoradiography.

(C) Schematic representations of UHRF1 and its functional domains (top). Each GST-fusion domain of UHRF1 was tested as a substrate for acetylation by PCAF (bottom).

(D) PCAF was transfected into HCT116 cells. The cell lysates were subjected to IP with anti-UHRF1 antibodies and immunoblotted with anti-acetyl-lysine antibodies.

(legend continued on next page)

suggested that PCAF directs acetylation of UHRF1 *in vivo*, supporting the interaction between two proteins (Figure S1A). Importantly, we showed that endogenous acetylation of UHRF1 was increased in the presence of FLAG-PCAF in HCT116 cells (Figure 1E). Moreover, both knockdown (KD) and inhibition of PCAF showed the decrease of UHRF1 acetylation, suggesting that PCAF mediates the acetylation of UHRF1 (Figures S1B–S1D). As our primary interest was in the effect of UHRF1 acetylation on hemi-methylated DNA binding, we focused on the SRA domain, which directly binds to hemi-methylated DNA. As prediction of PCAF substrates using the ASEB (Acetylation Set Enrichment Based method) and GPS-PAIL (GPS Prediction of Acetylation on International Lysines) programs showed that K490, K546, and K592 inside SRA domain could be acetylated by PCAF, we generated recombinant UHRF1 mutants in which each lysine was replaced with arginine and showed that only the acetylation level was decreased in K490R, indicating that K490 is the major acetylation site in UHRF1 (Figures 1E and 1F) (Li et al., 2006). To further assess the acetylation residue by PCAF, peptide bearing amino acids 485–495 of UHRF1 was acetylated by PCAF *in vitro* and analyzed by dot blot and mass spectrometry (Figure S1F). Especially in mass spectrometry, non-acetylated UHRF1 peptide had its main peak at 1,246.6 Da without PCAF, while the acetylated peptides appeared at 1,288.6 Da, with the 42 Da mass of K^+ incorporated (Figure 1G). When we co-transfected PCAF and UHRF1 wild-type (WT) or UHRF1 K490R into UHRF1 KD stable cells, we could detect a decrease in acetylation of UHRF1 in UHRF1 K490R-expressing cells (Figure 1H). Taken together, these data demonstrate that residue K490 in the SRA domain of UHRF1 is the major acetylated residue by PCAF.

Acetylation of UHRF1 Disrupts Hemi-methylated DNA Binding

To understand the significance of UHRF1 acetylation at K490, we compared the proximal sequence of human UHRF1 with the sequences of UHRF1 from other species and found that UHRF1 is highly conserved around K490 (Figure 2A). Next, we tested whether acetylation at K490 could affect the binding affinity of UHRF1 to hemi-methylated DNA. We performed electrophoretic mobility shift assays (EMSAs) and compared the DNA binding affinity of WT UHRF1 with acetyl-mimetic or acetyl-deficient mutants of UHRF1. Surprisingly, only the substitution of 490 lysine to glutamine mimicking acetyl-lysine (K490Q), totally abolished binding between UHRF1 and hemi-methylated DNA. Other substitutions in the SRA domain had no effect on hemi-methylated DNA binding (Figure 2B). To further evaluate the effect of UHRF1 acetylation on hemi-methylated DNA binding, we performed EMSA using UHRF1 fragment after *in vitro* acetylation assay. Results indicated that UHRF1 acetylation mediated by PCAF abrogated UHRF1 binding of hemi-methylated DNA (Figure S2A).

To obtain structural insights into this inhibition, we modeled the interaction between the SRA domain from UHRF1 and hemi-methylated DNA. In the NKR sequence, N489 and R491 seem to exhibit strong direct binding between the residue and the backbone of the DNA and K490 seems to have only long-distance interaction with the phosphate backbone of the DNA. These results suggest that acetylation of K490 only slightly weakens the interaction between the SRA domain and hemi-methylated DNA. However, our structural modeling suggests a flat conformation of the DNA binding loop (R484-G495), which may be stabilized by an ionic interaction between K490 and D485, and this solidified flat structure may be important in the binding affinity of the SRA domain for hemi-methylated DNA (Figure 2C). As our model suggested that this unique structure may be critical for the binding of the NKR finger to the hemi-methylated DNA surface, we tested whether the interaction between K490 and D485 is critical for hemi-methylated DNA binding affinity. We generated an UHRF1 mutant in which the 485th aspartic acid was replaced by asparagine and compared the DNA binding affinity of UHRF1 D485N to UHRF1 WT using EMSA. Binding of SRA to hemi-methylated DNA was significantly reduced suggesting that the ionic interaction between K490 and D485 is indeed critical to SRA function. Furthermore, we substituted 490th lysine of UHRF1 to another charge-neutral polar residues, N (Asn) to exclude the loss of positive charge effect of K490Q mutation and showed strong binding to hemi-methylated DNA (Figure 2D). Taken together, our results show that acetylation of K490 by PCAF disrupts the interaction between K490 and D485 and destabilizes the flat structure of the DNA binding loop, which results in inhibition of SRA binding to hemi-methylated DNA.

Acetylation of UHRF1 Attenuates Its Chromatin Association

Since we examined the structure around the NKR fingers and showed that acetylation of UHRF1 at K490 impairs its hemi-methylated DNA binding activity (Figures 2A–2D), we further explored the correlation between acetylation of UHRF1 and hemi-methylated binding affinity *in vivo* by assessing the chromatin association of UHRF1. First, we showed that chromatin association was enhanced in PCAF KD cells, compared to control cells (Figures S1D and S1E). To further confirm the direct effect of UHRF1 acetylation on chromatin recruitment, we generated WT or acetylation mutant UHRF1 (UHRF1 K490R, UHRF1 K490Q)-overexpressing cells, in which exogenous UHRF1 was integrated into the genome and endogenous UHRF1 was knocked down with short hairpin RNA (shRNA) (Figure 2E). We observed that UHRF1 with an K490Q could not bind to chromatin, while both WT and K490R were enriched in chromatin (Figure 2F). Collectively, these data suggest that acetylation of UHRF1 inhibits hemi-methylated DNA binding and its recruitment to chromatin, which is responsible for the maintenance of DNA methylation patterns after DNA replication.

(E and F) GST-fusion SRA domain of UHRF1 mutants incubated with PCAF and [^{14}C]-acetyl-CoA (E) or acetyl-coenzyme A (F) were visualized using autoradiography (E) and anti-acetyl-lysine antibody (F).
(G) Mass spectrometric analysis of UHRF1 following an acetylation assay using either GST or PCAF.
(H) HCT116 shUHRF1 cells overexpressing PCAF and UHRF1 WT or UHRF1 K490R were used to measure the acetylation level of UHRF1 at residue K490.

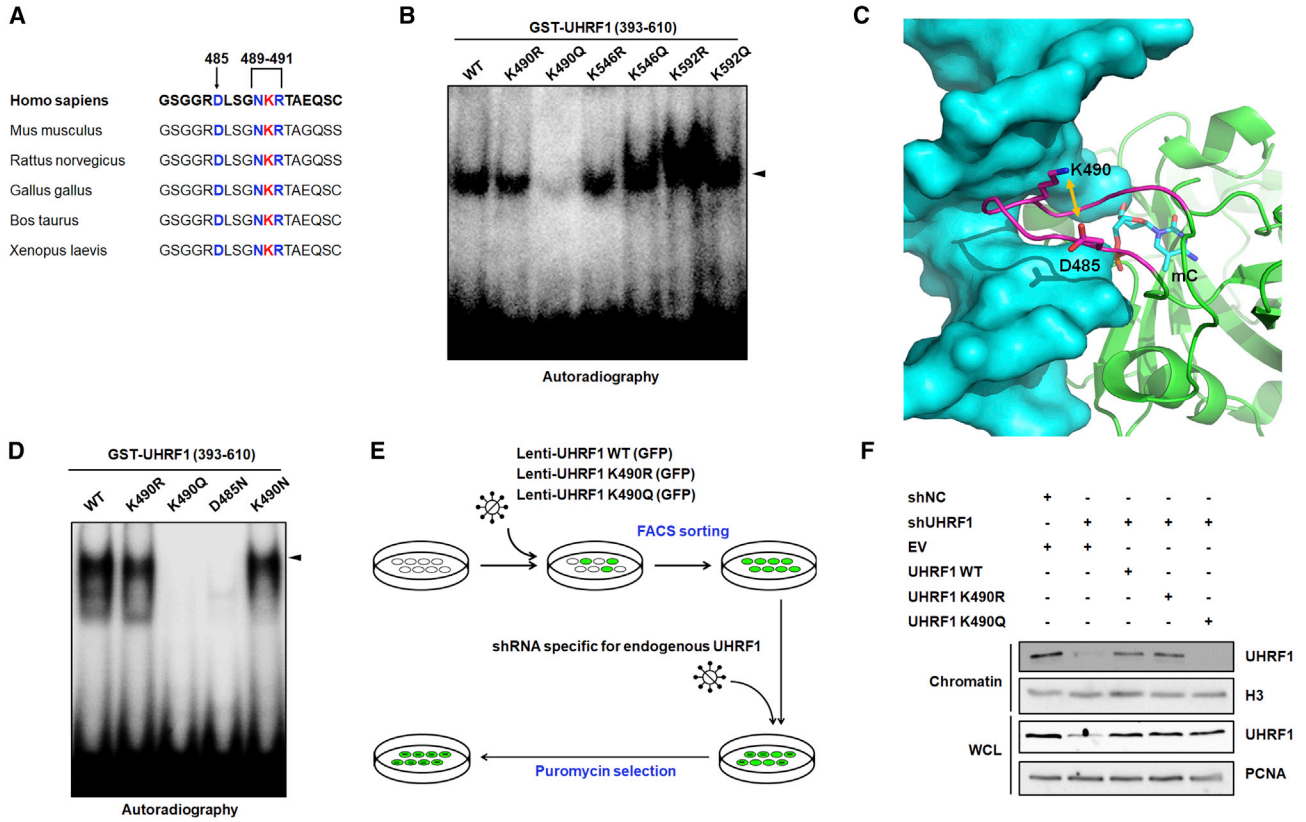

Figure 2. Acetylation of UHRF1 Reduces Binding Affinity for Hemi-methylated DNA

(A) Alignment of sequences from UHRF1 homologs of other species adjacent to human UHRF1 K490.

(B) EMSA to determine specificity of UHRF1 binding to DNA. Each acetylation target lysine mutant of UHRF1 was incubated with [^{32}P]-labeled hemi-mCpG duplexes.

(C) Flat conformation of the DNA binding loop (Arg484-Qln495, magenta), potentially stabilized by ionic interactions between K490 and D485 (yellow arrow). The DNA is shown using a surface representation (cyan), and UHRF1 in a ribbon representation (green). The bulged methyl cytosine, K490, and D485 are represented with a stick. This figure was developed from PDB code: 3F8I.

(D) For EMSA, each recombinant UHRF1 construct was incubated with [^{32}P]-labeled hemi-mCpG duplexes.

(E) Schematic for the generation of UHRF1 mutant stable cell lines. Exogenous UHRF1-overexpressing GFP-positive cells were sorted using fluorescence-activated cell sorting and knocked down by shRNA against UHRF1.

(F) HCT116 cells were arrested at the G1/S boundary and then released to S phase for 3 h. The chromatin fraction and whole-cell lysates were extracted, and the UHRF1 level was measured by western blots.

HDAC1 Catalyzes the Deacetylation of UHRF1 during S Phase

To better understand the delicate regulation of UHRF1 acetylation, we tested HDAC inhibitors in HCT116 cells and were able to show that UHRF1 acetylation was enhanced after treatment with trichostatin A (TSA) or sodium butyrate (NaBu) but not with nicotinamide (Figures 3A and S3A). As treatment of TSA or NaBu increased the acetylation of UHRF1, we sought to identify deacetylase involved in UHRF1 deacetylation. Since cell-cycle-dependent interaction between UHRF1 and HDAC1 has been reported, we examined whether HDAC1 could deacetylate UHRF1 (Unoki et al., 2004). HDAC1 or HDAC2 was ectopically expressed in HCT116 cells, but only HDAC1 promoted deacetylation of UHRF1 (Figure 3B). Next, we generated HDAC1 stably KD cell line and observed an increase in acetylation level of UHRF1 (Figure S3B). The interaction of two proteins peaked at 2 h after release to S phase, consistent with the results of previous studies (Figure 3C). Interestingly, UHRF1 acetylation levels decreased in the middle of S phase, adding convincing evidence that HDAC1 regulates UHRF1 acetylation in a cell-cycle-dependent manner (Figure 3D). To further identity the deacetylase activity of HDAC1 on UHRF1 K490, the K490R mutant was ectopically expressed in control and HDAC1 KD cells, and its acetylation levels were measured. The UHRF1 K490R mutant exhibited a significantly reduced acetylation level, and it did not increase in HDAC1 KD cells, compared to UHRF1 WT (Figure 3E). Since HDAC1 promotes deacetylation of UHRF1 at K490 during S phase, we further investigated how HDAC1 affects hemi-methylated DNA binding of UHRF1 *in vivo*. We first measured the chromatin-bound UHRF1 and identified that UHRF1 is actively recruited to chromatin during the S phase. However, even in S phase, UHRF1 showed reduced chromatin binding in HDAC1 KD cells, indicating that UHRF1 deacetylation by HDAC1 is a prerequisite for chromatin association (Figure 3F).

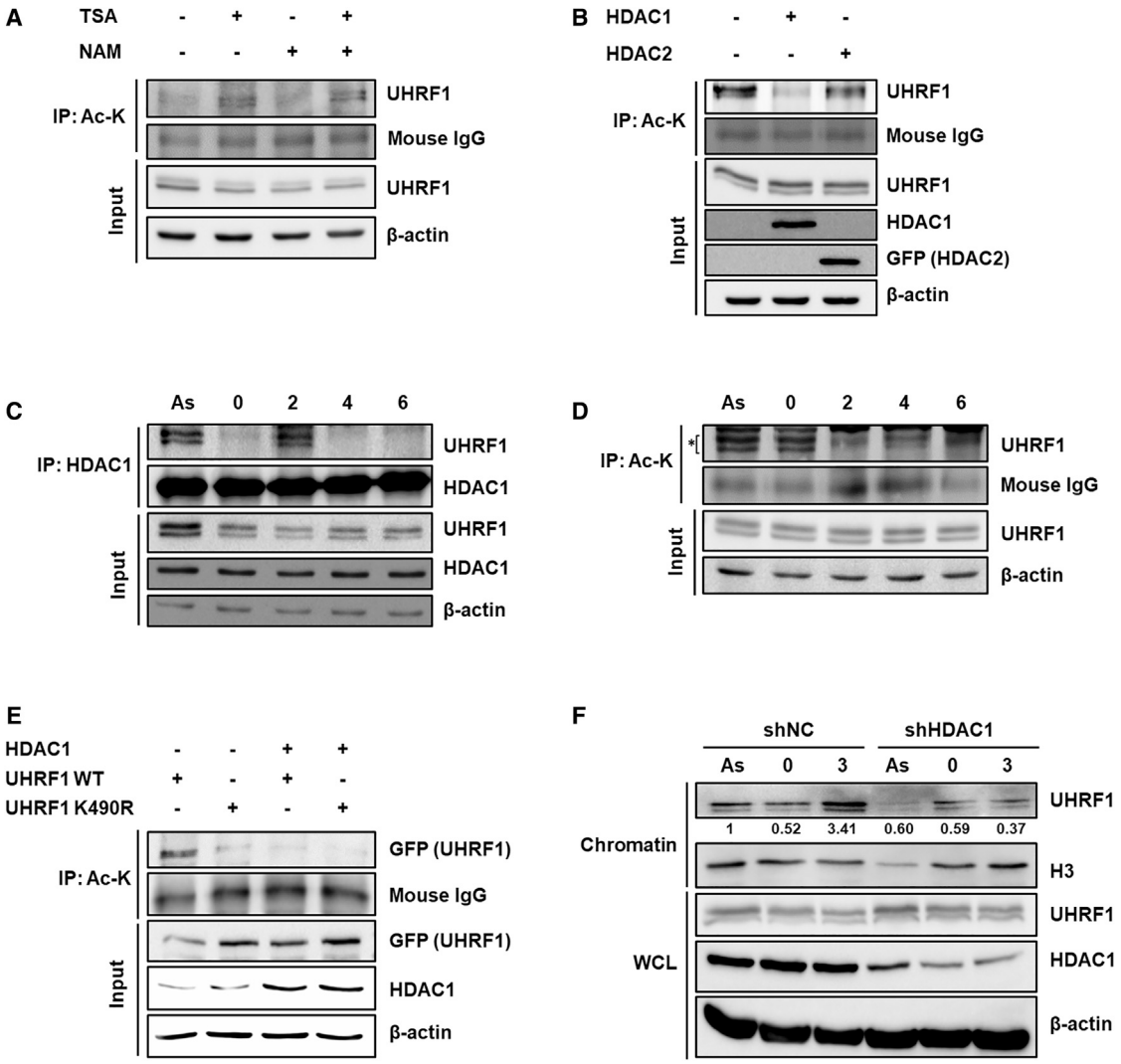

Figure 3. HDAC1 Deacetylates UHRF1 K490

(A) HCT116 cells treated with TSA or nicotineamide (NAM) for 12 h were immunoprecipitated using anti-acetyl-lysine antibodies and evaluated by western blots.

(B) HDAC1 or HDAC2 was transfected into HCT116 cells. The cell lysates were immunoprecipitated using anti-acetyl-lysine antibodies and immunoblotted with anti-UHRF1 antibodies.

(C and D) HCT116 cells were arrested at the G1/S boundary and then released into S phase. The interaction between UHRF1-HDAC1 (C) and level of UHRF1 acetylation (D) were analyzed by IP assay. * represents acetylated UHRF1.

(E) shUHRF1 cells overexpressing HDAC1 and UHRF1 WT or K490R were used to measure the acetylation level of UHRF1 at K490.

(F) HCT116 shNC and shHDAC1 cells were arrested at the G1/S boundary and then released to S phase for 3 h. The UHRF1 level in chromatin and whole-cell lysates was measured by western blots.

Altogether, our data showed that HDAC1 deacetylates UHRF1 at K490 in cell-cycle-dependent manner, which is required for UHRF1 to bind hemi-methylated DNA and be recruited to chromatin.

Acetylation of UHRF1 at K490 Disrupts the Inheritance of Global DNA Methylation Patterns and Results in Transcriptome Changes

Since we found that acetylation of UHRF1 abrogates hemi-methylated DNA binding, we next examined the effect of UHRF1 acetylation on the maintenance of genome-wide DNA methylation patterns. To explore this, gene body, promoter, and intergenic DNA methylation profiles were measured by Illumina Infinium Methylation EPIC array in endogenous UHRF1-depleted HCT116 cells replaced with indicated mutants. As expected, UHRF1-depleted cells recovered with UHRF1 WT or UHRF1 K490R restored DNA methylation. However, restoration with UHRF1 K490Q was incapable of maintaining global DNA methylation patterns, with its results being more similar to cells with no UHRF1 rescue (Figure 4A). To further understand this global hypomethylation, we analyzed differentially methylated CpG probes using the

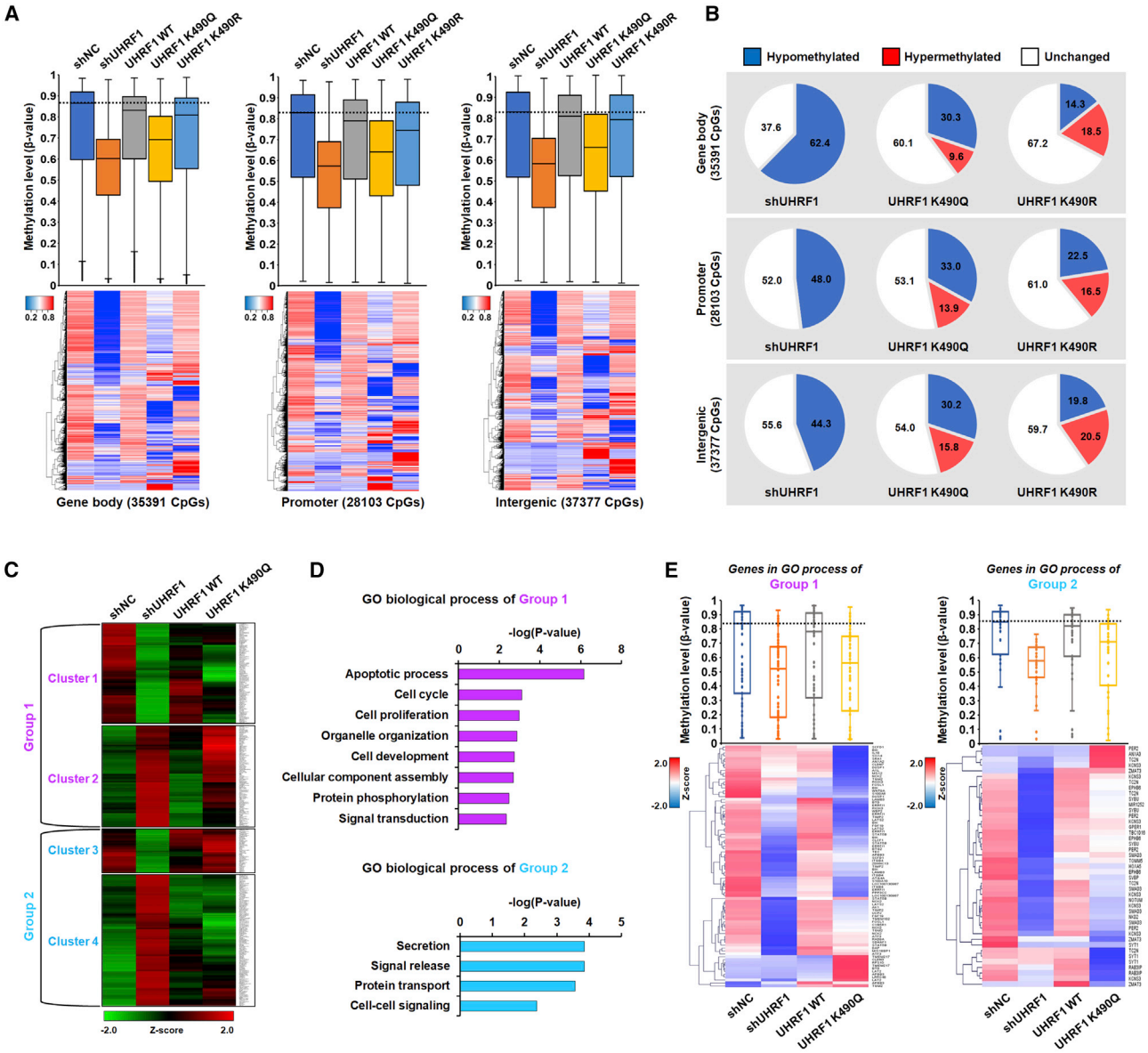

Figure 4. Acetylation of UHRF1 Disrupts DNA Methylation Maintenance and Alters Gene Expression

(A) Global DNA methylation profiles, measured by Illumina Infinium Methylation EPIC arrays, of genomic DNA from endogenous UHRF1-depleted HCT116 cells reconstituted with WT or mutants of UHRF1. All array probes for each sample were used to generate box and whisker plots (top) and heatmaps (bottom). Whisker plots represent the 25th–75th percentiles, with midlines indicating median values. Whiskers extend to the minimum/maximum value of the data, including outliers (black circles). The horizontal dash lines in each boxplots represent the median β values in shNC.

(B) Pie graphs representing the proportion of unchanged, hypomethylated, and hypermethylated CpG probes in each gene, promoter, and intergenic region of the genome.

(C) Heatmap of gene-expression *Z* scores computed for genes that are differentially expressed (fold change >1.5) between control and UHRF1 KD cells.

(D) GO terms of genes in group 1 and group 2 were analyzed in gene ontology consortium. x axis represents the adjusted p value transformed by –log10, and y axis denotes the enriched GO terms.

(E) DNA methylation profiles of genes in GO processes of each group were presented boxplots (top) and heatmaps (bottom). Heatmap of DNA methylation *Z* score computed for promoter CpGs of genes in GO processes of each group.

CpG location as a mark. We observed that hypomethylation was significantly more common in UHRF1-depleted cells. Intriguingly, around 30% of CpGs were hypomethylated in UHRF1 K490Q cells , exhibiting global DNA hypomethylation. However, UHRF1 K490R showed similar percentages to WT UHRF1 for both hyper and hypomethylated CpGs in all regions (Figure 4B).

Since DNA methylation affects not only genomic integrity but also transcriptional regulation, we next explored UHRF1-associated transcriptome profiles to investigate whether UHRF1

acetylation could alter gene-expression patterns. UHRF1 KD and UHRF1 K490Q-restored cells showed dramatic changes in gene expression, whereas their patterns are largely retained when UHRF1 WT are recovered. We classified genes into four clusters, depending on correlation of gene-expression patterns in each cell. Group 1, which exhibit similar gene-expression patterns in UHRF1 KD and UHRF1 K490Q-restored cells, was classified as a group of genes controlled by UHRF1-hemi-methylated DNA binding, with group 2 being regulated independently (Figure 4C). Interestingly, gene ontology (GO) term analysis showed that genes in group 1 were related to cell survival including apoptosis and cell proliferation, whereas genes in group 2 were associated with secretion or signaling processes (Figure 4D). Combining DNA methylation and gene-expression profiling data, we identified that genes included in group 1 GO process showed consistent DNA methylation patterns between UHRF1 KD and UHRF1 K490Q-restored cells, indicating that their expressions are dependent on hemi-methylated DNA binding affinity and DNA methylation status in each cell. On the other hand, gene-expression and DNA methylation patterns of genes in group 2 were not correlated in UHRF1 KD and UHRF1 K490Q-recovered cells (Figures 4E, S4A, and S4B). These combined data indicated that hemi-methylated DNA binding of UHRF1 is essential to regulate DNA methylation of cell survival-related genes for their transcription.

Taken together, genome-wide DNA methylation and transcriptome profiling data show that regulation of UHRF1 acetylation is sufficient to disrupt genomic DNA methylation maintenance after DNA replication and regulates expression of genes associated with cell survival.

DISCUSSION

The inheritance of epigenetic information is essential for cell survival and the maintenance of cellular identity. As one of the main epigenetic regulators for the maintenance of DNA methylation, hemi-methylated DNA binding of UHRF1 is critical for replication of DNA methylation patterns.

In this study, we discovered that UHRF1 is acetylated at K490 by PCAF, which resides in the NKR finger of the SRA domain and showed that this acetylation disrupts its binding of hemi-methylated DNA. Structural modeling and EMSA analyses revealed that interactions between two amino acids, K490 and D485, of UHRF1 are also important for hemi-methylated DNA binding.

Interestingly, differential hemi-methylated DNA binding affinities for UHRF1 and UHRF2 provide additional evidence of the importance of interaction between D485 and K490 in UHRF1 affinity for hemi-methylated DNA. Although UHRF2 is highly homologous to UHRF1 in sequence and structure, the sequence alignment shows that UHRF1 D485 is substituted with Asn(N) in UHRF2 (Figure S4C). Since UHRF2 has no Asp(D) to create the flat structure with lysine in the NKR finger, it is expected to show weaker binding to hemi-methylated DNA. In fact, UHRF1 displays at least a 10-fold stronger binding affinity for hemi-methylated DNA when compared to UHRF2, indicating that the interaction K490-D485 is critical for UHRF1 binding to hemi-methylated DNA (Vaughan et al., 2018).

For decades, studies have shown that aberrant expression of UHRF1 is highly correlated to aggressiveness in certain types of tumors, implying a correlation between overexpression of UHRF1 and abnormal DNA hypermethylation (Liang et al., 2015; Liu et al., 2017). Recent studies on the novel mechanism of UHRF1 binding to hemi-methylated DNA suggest that the SRA domain may be a promising therapeutic target for cancer therapies (Kong et al., 2019; Polepalli et al., 2019). However, a finer understanding of the regulatory mechanism explaining the importance of the SRA domain in cancer cell proliferation needs further investigation.

Here, we found that cells recovered with UHRF1 K490Q exhibited global DNA hypomethylation, indicating that disruption in interaction between UHRF1 and hemi-methylated DNA by UHRF1 acetylation could relieve aberrant DNA hypermethylation of cancer cells. However, the methylation EPIC array showed that KD of HDAC1 does not alter global DNA methylation, even though it promotes UHRF1 acetylation at K490 (Figures S3B, S4D, and S4E). We think that it might come from a technical limitation of bisulfite conversion-based DNA methylation analysis, which could not distinguish between 5mC and demethylating 5mC marker, 5hmC. HDAC1 inhibition could increase TET2 activity and also global 5hmC level (Zhang et al., 2017), while simultaneously promoting acetylation of UHRF1. It might be interpreted as "no change" in DNA methylation. However, further studies overcoming this technical limitation are needed to definitively demonstrate the regulatory mechanism of UHRF1 acetylation-dependent DNA methylation.

Finally, we also observed that substitution of K490 to acetyl-mimetic Q altered gene-expression patterns. Combining DNA methylation array and gene-expression profiling, our data suggest that UHRF1 acetylation might control cell survival by regulating DNA methylation levels.

As UHRF1 forms a complex with various proteins in S phase, regulation of UHRF1 acetylation by PCAF and HDAC1 might not be a sole regulatory mechanism of UHRF1-mediated DNA methylation. Our findings suggest that induction of UHRF1 acetylation could abolish abnormal DNA hypermethylation in certain types of cancer and propose that this mechanism could be a novel approach for the treatment of these cancers.

STAR★METHODS

Detailed methods are provided in the online version of this paper and include the following:

- KEY RESOURCES TABLE
- RESOURCE AVAILABILITY
  - Lead Contact
  - Materials Availability
  - Data and Code Availability
- EXPERIMENTAL MODEL AND SUBJECT DETAILS
  - Cell lines
- METHOD DETAILS
  - Details on antibody and reagent usage
  - Constructs and siRNAs
  - Stable knockdown cell lines
  - Immunoprecipitation assays

- *In vitro* acetylation assay
- Electrophoretic mobility shift assay
- Liquid chromatography–mass spectrometry
- Chromatin isolation
- Genome-wide DNA methylation profiling

● QUANTIFICATION AND STATISTICAL ANALYSIS

SUPPLEMENTAL INFORMATION

Supplemental Information can be found online at https://doi.org/10.1016/j.celrep.2020.107958.

ACKNOWLEDGMENTS

We appreciate Jaewon Kim (Ewha Womans University) for methylation profile analysis. This work was supported by National Research Foundation of Korea (NRF) grant, Ministry of Science, ICT & Future Planning (NRF-2013R1A2A2A01068788, 2019R1A4A2001609). J.Y.H. was supported from the Global Ph.D Fellowship funded by NRF (NRF-2015H1A2A1033488). Funding for open access charge: NRF of Korea (2019R1A4A2001609).

AUTHOR CONTRIBUTIONS

Conceptualization, J.Y.H. and S.-B.S.; Methodology, J.Y.H. and S.-B.S.; Validation, J.Y.H., J.W.P., J.-Y. Kang and J.P.; Formal Analysis, N.-C.H.; Investigation, J.Y.H., J.W.P., J.-Y. Kang, and J.P.; Resources, C.-H.K., J.-Y. Kim, and J.-W.K.; Writing, J.Y.H. and S.B.S.; Supervision, S.B.S.; Project Administration, S.B.S.; Funding Acquisition, J.Y.H. and S.B.S.

DECLARATION OF INTERESTS

The authors declare no competing interests.

Received: January 29, 2020
Revised: May 14, 2020
Accepted: July 2, 2020
Published: July 28, 2020

REFERENCES

Arita, K., Ariyoshi, M., Tochio, H., Nakamura, Y., and Shirakawa, M. (2008). Recognition of hemi-methylated DNA by the SRA protein UHRF1 by a base-flipping mechanism. Nature *455*, 818–821.

Avvakumov, G.V., Walker, J.R., Xue, S., Li, Y., Duan, S., Bronner, C., Arrowsmith, C.H., and Dhe-Paganon, S. (2008). Structural basis for recognition of hemi-methylated DNA by the SRA domain of human UHRF1. Nature *455*, 822–825.

Bostick, M., Kim, J.K., Estève, P.O., Clark, A., Pradhan, S., and Jacobsen, S.E. (2007). UHRF1 plays a role in maintaining DNA methylation in mammalian cells. Science *317*, 1760–1764.

Chuang, L.S., Ian, H.I., Koh, T.W., Ng, H.H., Xu, G., and Li, B.F. (1997). Human DNA-(cytosine-5) methyltransferase-PCNA complex as a target for p21WAF1. Science *277*, 1996–2000.

Frauer, C., Hoffmann, T., Bultmann, S., Casa, V., Cardoso, M.C., Antes, I., and Leonhardt, H. (2011). Recognition of 5-hydroxymethylcytosine by the Uhrf1 SRA domain. PLoS ONE *6*, e21306.

Hahm, J.Y., Kim, J.Y., Park, J.W., Kang, J.Y., Kim, K.B., Kim, S.R., Cho, H., and Seo, S.B. (2019). Methylation of UHRF1 by SET7 is essential for DNA double-strand break repair. Nucleic Acids Res. *47*, 184–196.

Hashimoto, H., Horton, J.R., Zhang, X., Bostick, M., Jacobsen, S.E., and Cheng, X. (2008). The SRA domain of UHRF1 flips 5-methylcytosine out of the DNA helix. Nature *455*, 826–829.

Irizarry, R.A., Ladd-Acosta, C., Carvalho, B., Wu, H., Brandenburg, S.A., Jeddeloh, J.A., Wen, B., and Feinberg, A.P. (2008). Comprehensive high-throughput arrays for relative methylation (CHARM). Genome Res. *18*, 780–790.

Kang, J.Y., Kim, J.Y., Kim, K.B., Park, J.W., Cho, H., Hahm, J.Y., Chae, Y.C., Kim, D., Kook, H., Rhee, S., et al. (2018). KDM2B is a histone H3K79 demethylase and induces transcriptional repression via sirtuin-1-mediated chromatin silencing. FASEB J. *32*, 5737–5750.

Kim, K.B., Son, H.J., Choi, S., Hahm, J.Y., Jung, H., Baek, H.J., Kook, H., Hahn, Y., Kook, H., and Seo, S.B. (2015). H3K9 methyltransferase G9a negatively regulates UHRF1 transcription during leukemia cell differentiation. Nucleic Acids Res. *43*, 3509–3523.

Kong, X., Chen, J., Xie, W., Brown, S.M., Cai, Y., Wu, K., Fan, D., Nie, Y., Yegnasubramanian, S., Tiedemann, R.L., et al. (2019). Defining UHRF1 Domains that Support Maintenance of Human Colon Cancer DNA Methylation and Oncogenic Properties. Cancer Cell *35*, 633–648.

Kulis, M., and Esteller, M. (2010). DNA methylation and cancer. Adv. Genet. *70*, 27–56.

Li, A., Xue, Y., Jin, C., Wang, M., and Yao, X. (2006). Prediction of Nepsilon-acetylation on internal lysines implemented in Bayesian Discriminant Method. Biochem. Biophys. Res. Commun. *350*, 818–824.

Liang, D., Xue, H., Yu, Y., Lv, F., You, W., and Zhang, B. (2015). Elevated expression of UHRF1 predicts unfavorable prognosis for patients with hepatocellular carcinoma. Int. J. Clin. Exp. Pathol. *8*, 9416–9421.

Liu, X., Gao, Q., Li, P., Zhao, Q., Zhang, J., Li, J., Koseki, H., and Wong, J. (2013). UHRF1 targets DNMT1 for DNA methylation through cooperative binding of hemi-methylated DNA and methylated H3K9. Nat. Commun. *4*, 1563.

Liu, X., Ou, H., Xiang, L., Li, X., Huang, Y., and Yang, D. (2017). Elevated UHRF1 expression contributes to poor prognosis by promoting cell proliferation and metastasis in hepatocellular carcinoma. Oncotarget *8*, 10510–10522.

Méndez, J., and Stillman, B. (2000). Chromatin association of human origin recognition complex, cdc6, and minichromosome maintenance proteins during the cell cycle: assembly of prereplication complexes in late mitosis. Mol. Cell. Biol. *20*, 8602–8612.

Oh, S.T., Kim, K.B., Chae, Y.C., Kang, J.Y., Hahn, Y., and Seo, S.B. (2014). H3K9 histone methyltransferase G9a-mediated transcriptional activation of p21. FEBS Lett. *588*, 685–691.

Polepalli, S., George, S.M., Valli Sri Vidya, R., Rodrigues, G.S., Ramachandra, L., Chandrashekar, R., M, D.N., Rao, P.P.N., Pestell, R.G., and Rao, M. (2019). Role of UHRF1 in malignancy and its function as a therapeutic target for molecular docking towards the SRA domain. Int. J. Biochem. Cell Biol. *114*, 105558.

Sharif, J., Muto, M., Takebayashi, S., Suetake, I., Iwamatsu, A., Endo, T.A., Shinga, J., Mizutani-Koseki, Y., Toyoda, T., Okamura, K., et al. (2007). The SRA protein Np95 mediates epigenetic inheritance by recruiting Dnmt1 to methylated DNA. Nature *450*, 908–912.

Unoki, M., Nishidate, T., and Nakamura, Y. (2004). ICBP90, an E2F-1 target, recruits HDAC1 and binds to methyl-CpG through its SRA domain. Oncogene *23*, 7601–7610.

Vaughan, R.M., Dickson, B.M., Cornett, E.M., Harrison, J.S., Kuhlman, B., and Rothbart, S.B. (2018). Comparative biochemical analysis of UHRF proteins reveals molecular mechanisms that uncouple UHRF2 from DNA methylation maintenance. Nucleic Acids Res. *46*, 4405–4416.

Zhang, J., Gao, Q., Li, P., Liu, X., Jia, Y., Wu, W., Li, J., Dong, S., Koseki, H., and Wong, J. (2011). S phase-dependent interaction with DNMT1 dictates the role of UHRF1 but not UHRF2 in DNA methylation maintenance. Cell Res. *21*, 1723–1739.

Zhang, Y.W., Wang, Z., Xie, W., Cai, Y., Xia, L., Easwaran, H., Luo, J., Yen, R.C., Li, Y., and Baylin, S.B. (2017). Acetylation Enhances TET2 Function in Protecting against Abnormal DNA Methylation during Oxidative Stress. Mol. Cell *65*, 323–335.

STAR★METHODS

KEY RESOURCES TABLE

REAGENT or RESOURCE	SOURCE	IDENTIFIER
Antibodies		
Rabbit normal IgG Control	Merck Millipore	Cat# 12-370; RRID: AB_145841
Mouse normal IgG Control	Merck Millipore	Cat# 12-371; RRID: AB_145840
Mouse monoclonal anti-Ac-lysine (7F8)	Santa Cruz Biotechnology	Cat# sc-81623; RRID: AB_1118639
Rabbit polyclonal anti-acetyl-Lysine	Abcam	Cat# ab21623; RRID: AB_446436
Mouse monoclonal anti-UHRF1 (H-8)	Santa Cruz Biotechnology	Cat# sc-373750; RRID: AB_10947236
Mouse monoclonal ANTI-FLAG® M2	Sigma-Aldrich	Cat# F3165; RRID: AB_259529
Mouse monoclonal anti-GFP (B-2)	Santa Cruz Biotechnology	Cat# sc-9996; RRID: AB_627695
Mouse monoclonal anti-PCAF (E-8)	Santa Cruz Biotechnology	Cat# sc-13124; RRID: AB_2128417
Mouse monoclonal anti-β-Actin	Santa Cruz Biotechnology	Cat# sc-47778; RRID: AB_626632
Mouse monoclonal anti-Histone H3	Merck Millipore	Cat# 05-499; RRID: AB_309763
Mouse monoclonal anti-PCNA (PC10)	Santa Cruz Biotechnology	Cat# sc-56; RRID: AB_628110
Mouse monoclonal anti-HDAC1	Upstate	Cat# 05-614
Bacterial and Virus Strains		
BL21	Invitrogen	Cat# C601003
DH5α	Invitrogen	Cat# 18265017
Chemicals, Peptides, and Recombinant Proteins		
Tris base	Glentham	GP7166
HCl	DUKSAN	1129
NaCl	DUKSAN	81
KCl	DUKSAN	370
Nonidet P-40/IGEPAL® CA-630	Sigma-Aldrich	I3021
EDTA	Life Science	105
EGTA	Sigma-Aldrich	E4378
Xpert Protease Inhibitor Cocktail Solution	Gendepot	P3100
Triton X-100	Sigma-Aldrich	T8787
Phenylmethylsulfonyl fluoride	Biosesang	P1021
Puromycin	Sigma-Aldrich	P8833
Polybrene	Sigma-Aldrich	H9268
RPMI medium 1640 (RPMI)	GIBCO	23400-021
Dulbecco's Modified Eagle Medium (DMEM)	GIBCO	12800-017
Fetal Bovine Serum (FBS), Qualified	GIBCO	12483-020
Penicillin/Streptomycin	Welgene	LS202-02
Dulbecco's phosphate buffered saline (DPBS)	Welgene	LB001-02
Trypsin-EDTA solution	Welgene	LS015-08
Lipofectamine® 2000 Reagent	Invitrogen	11668-019
Glutathione Sepharose® 4B	GE Healthcare	17-0756-01
ATP Disodium Trihydrate	AMRESCO	0220
Adenosine 5′-Triphosphate, [γ −32P]	PerkinElmer	NEG502Z
Protein A/G-Agarose	Gendepot	P9203
IPTG	Duchefa Biochemie	I1401
DITHIOTHREITOL	Duchefa Biochemie	D1309
L-glutatione reduced	Sigma-Aldrich	G4251

(*Continued on next page*)

Continued

REAGENT or RESOURCE	SOURCE	IDENTIFIER
Bovine Serum Albumin	CellNest	CNB102-0100
Glycerol	JUNSEI	27210-0350
HEPES	GENOMICBASE	HEP001
Boric acid	DUKSAN	1004
Acetyl coenzyme A, [ACETYL-1-14C]	PerkinElmer	NEC313
Acetyl coenzyme A sodium salt	Sigma-Aldrich	A2056
Brilliant Blue R	Sigma-Aldrich	27816
Acetic acid	JUNSEI	31010-0350
Methanol	Merck Millipore	106009
Ethanol	Merck Millipore	100983
Glycine	Glentham	GM2385
Ampicillin, sodium salt	MP Biomedicals	190148
Kanamycin sulfate	AMRESCO	408
Tryptone	Duchefa Biochemie	T1332
Magnesium chloride solution	Sigma-Aldrich	M1028
Magnesium sulfate	Sigma-Aldrich	M7506
Sodium dodecyl sulfate (SDS)	Duchefa Biochemie	S1377
Sodium deoxycholate (SDC)	Sigma-Aldrich	D6750
Polyethylenimine, Linear	Polyscience	23966
Sodium butyrate	Sigma-Aldrich	303410
Bromophenol Blue	JUNSEI	65305-0310
Ammonium persulfate	Sigma-Aldrich	A3678
Acrylamide/bis solution	BIOTAPS	AS05-1
T4 Polynucleotide Kinase	New England Biolabs	M0201
Yeast extract	Duchefa Biochemie	Y1333
N,N,N',N'-Tetramethylethylene-Diamine	BIOWORLD	42000060-2
Sucrose	Duchefa Biochemie	S0809
Tri-RNA Reagent	Favorgen	FATRR 001
Chloroform	DUKSAN	D1268
2-Propanol	Merck Millipore	109634
Trichostatin A	Sigma-Aldrich	T8552
Nicotinamide	Sigma-Aldrich	N0636
Thymidine	Sigma-Aldrich	T9250
Ciprofloxacin	Cellgro	JG-61-277-RF
PCAF protein	Sigma-Aldrich	14-309
Critical Commercial Assays		
Wizard® Genomic DNA Purification Kit	Promega	A1120
FavorPrep Plasmid DNA Extraction Mini Kit	FAVOGEN	FAPDE 300
Deposited Data		
Genomic DNA methylation profiling data	This paper	GEO: GSE151865
Experimental Models: Cell Lines		
HCT116	Korean Cell Line Bank	10247
HEK293T	Korean Collection for Type Cultures (KCTC)	HC20005
K562	Korean Collection for Type Cultures (KCTC)	HC18102
Oligonucleotides		
shNC	(Hahm et al., 2019)	N/A
siNC	Bioneer	SN-1012
shUHRF1	(Hahm et al., 2019)	N/A

(*Continued on next page*)

Continued

REAGENT or RESOURCE	SOURCE	IDENTIFIER
shPCAF	This papar	N/A
siPCAF	Bioneer	SDH-1001(siRNA #8850-1,2,3)
shHDAC1	This papar	N/A
Recombinant DNA		
pCMV-3xflag-PCAF	This paper	N/A
pCMX-PCAF	(Oh et al., 2014)	N/A
pCMV-3xflag-UHRF1	(Hahm et al., 2019)	N/A
pGEX-4T2-UHRF1 WT	(Hahm et al., 2019)	N/A
pGEX-4T2-UHRF1 #1	(Hahm et al., 2019)	N/A
pGEX-4T2-UHRF1 #2	(Hahm et al., 2019)	N/A
pGEX-4T2-UHRF1 #3	(Hahm et al., 2019)	N/A
pGEX-4T2-UHRF1 #4	(Hahm et al., 2019)	N/A
pEGFP-UHRF1	(Hahm et al., 2019)	N/A
pEGFP-UHRF1 K490R	(Hahm et al., 2019)	N/A
pGEX-4T2-UHRF1 (393-610) K490R	This paper	N/A
pGEX-4T2-UHRF1 (393-610) K490Q	This paper	N/A
pGEX-4T2-UHRF1 (393-610) K546R	This paper	N/A
pGEX-4T2-UHRF1 (393-610) K546Q	This paper	N/A
pGEX-4T2-UHRF1 (393-610) K592R	This paper	N/A
pGEX-4T2-UHRF1 (393-610) K592Q	This paper	N/A
pGEX-4T2-UHRF1 (393-610) K490N	This paper	N/A
pGEX-4T2-UHRF1 (393-610) D485N	This paper	N/A
pLenti-puro	Addgene	39481
pLenti-GFP	This paper	N/A
pLenti-GFP/UHRF1 WT	This paper	N/A
pLenti-GFP/UHRF1 K490R	This paper	N/A
pLenti-GFP/UHRF1 K490Q	This paper	N/A
pCMX-HDAC1	(Kim et al., 2015)	N/A
pEGFP-HDAC2	(Kim et al., 2015)	N/A
pLKO.1-puro	Addgene	8453
p3XFLAG-CMV-10	(Kang et al., 2018)	N/A
Other		
Nitrocellulose Transfer Membrane	Pall Bio trace	A66485

RESOURCE AVAILABILITY

Lead Contact

Further information and requests for resources and reagents should be directed to and will be fulfilled by the Lead Contact, Sang-Beom Seo (sangbs@cau.ac.kr).

Materials Availability

This study did not generate new unique reagents.

Data and Code Availability

Illumina Infinium Methylation EPIC array datasets during this study are available at the Gene Expression Omnibus under code GEO. The accession number for the array data sets reported in this paper is GEO: GSE151865.

EXPERIMENTAL MODEL AND SUBJECT DETAILS

Cell lines

For generation of HCT116 cells stably expressing wild-type UHRF1, acetyl-deficient (K490R) or acetyl-mimetic UHRF1(K490Q), the vectors pLenti-GFP, pLenti-GFP/UHRF1, pLenti-GFP/UHRF1 K490R or pLenti-GFP/UHRF1 K490Q were transfected into HEK293T cells (KCTC; 10247) using polyethylenimine (PEI) (Polyscience; 23966). After 16 h, sodium butyrate was treated for 8 h, expected to improve the productivity of virus. After 16h, lentiviral supernatant was collected and used for the infection of HCT116 cells in combination with 8ug/mL polybrene (Sigma-Aldrich; H9268). After lentiviral infection of HCT116 cells, GFP positive cells were collected with fluorescence-actived cell sorting (FACS) method. HEK293T cell line was cultured in high glucose DMEM (GIBCO; 12800-017) with 0.3% HEPES (GENOMICBASE; HEP001), and HCT116, K562 and UHRF1 stably expressed HCT116 stable cells in RPMI (GIBCO; 23400-021) supplemented with 10% fetal bovine serum (FBS) (GIBCO; 12483-020) and 0.05% penicillin-streptomycin (Welgene; LS202-02), at 37°C in a 5% CO_2 atmosphere. G1/S synchronization was achieved by a double thymidine block. In brief, cells were cultured in the presence of 2.5 mM thymidine (Sigma-Aldrich; T9250) for 19 h, and then released to grow for 10 h. Cells were then treated for another 15 h with 2.5 mM thymidine, causing the cells to arrest at the G1/S boundary. The arrested cells were allowed to enter the S phase by washing the thymidine away with Dulbecco's phosphate buffered saline (DPBS) (Welgene; LB001-02).

METHOD DETAILS

Details on antibody and reagent usage

Rabbit normal IgG control antibody (Millipore; 12-370) was used for immunoblot shown in Figures S1A and S1B. Mouse normal IgG control antibody (Millipore; 12-371) was used for immunoblot shown in Figures 1A, 1D, 3A, 3B, 3D, 3E, and S3 and for immunoprecipitation shown in Figures 1A and 1D. Anti-acetyl-lysine (Santa Cruz Biotechnology; sc-81623) was used for immunoprecipitation shown in Figures 1A, 1G, 3A, 3B, 3D, and 3E and for immunoblot for Figure 1E; anti-acetyl-lysine (Abcam; ab21623) was used for immunoprecipitation shown in Figures S1A and S1B and for immunoblot for Figure S1D. Anti-UHRF1 (Santa Cruz Biotechnology; sc-373750) was used for immunoprecipitation shown in Figures 1A and 1F and for immunoblot shown in Figures 1A, 1E, 2F, 3A-3D, 3F, S1A, S1B, S2B, S2C, and S3. Anti- FLAG® M2 (Sigma Aldrich; F3165) was used for immunoblot and immunoprecipitation shown in Figure 1D. Anti-GFP (Santa Cruz Biotechnology; sc-9996) was used for immunoblot shown in Figures 1D, 1G, 3B, and 3E and immunoprecipitation shown in Figure 1D. Anti-PCAF (Santa Cruz Biotechnology; sc-13124) was used for immunoblot shown in Figures 1E, S1A, S1B, S2B, and S2C. Anti-β-Actin (Santa Cruz Biotechnology; sc-47778) was used for immunoblot shown in Figures 1E and 1F, 3A–3F, S1A, S1B, S2B, S2C, and S3. Anti-histone H3 (Merck Millipore; 05-499) was used for immunoblot shown in Figures 2F, 3F, S2B, and S2C. Anti-PCNA (Santa Cruz Biotechnology; sc-56) was used for immunoblot shown in Figure 2F. Anti-HDAC1 (Upstate; 05-614) was used for immunoblot shown in Figures 3B, 3C, 3E, 3F, and S3 and for immunoprecipitation shown in Figure 3C.

Lipofectamine® 2000 Reagent (Invitrogen; 11668-019) was used for transfection of siRNA in HCT116 cells. PEI was used for transfection in HCT116 or HEK293T cells. 500 nM or 1 μM of trichostatin A (TSA) or 10 mM of nicotineamide (NAM) was treated for 12 h in HCT116 cells.

Constructs and siRNAs

The full-length PCAF coding sequence was subcloned into p3XFLAG-CMV-10. cDNAs of GST-UHRF1 (393-610) single mutants (K490R, K490Q, K546R, K546Q, K592R, K592Q, K490N, D485N) were generated from GST-UHRF1(393-610) WT via two-step PCR (one pair of fully complementary primer). Sequences of all oligonucleotides used for amplification or mutagenesis PCRs are listed in Table S1. Human PCAF (AccuTarget Genome-wide Predesigned siRNA, SDH-1001) and control siRNAs (AccuTarget Negative Control siRNA, SN-1012) were obtained from Bioneer.

Stable knockdown cell lines

DNA oligonucleotides that encode UHRF1, HDAC1 and PCAF short hairpin RNA (shRNA) were as follows: for shUHRF1: 5′ - CCGGAGATATAACGTTAGGGTTTCTCGAGAAACCCTAACGTTATATCTTTTTTG - 3′, for shHDAC1: 5′ – CCGGCCTAATGAGCTTCCATACAATCTCGAGATTGTATGGAAGCTCATTAGGTTTTTG - 3′, for shPCAF: 5′ – CCGGGCAGATACCAAACAAGTTTATCTCGAGATAAACTTGTTTGGTATCTGCTTTTTG - 3. These oligonucleotides were inserted into the AgeI/EcoRI site of the pLKO.1 TRC vector (Addgene; 8453) according to standard procedures. To produce virus particles, 293T cells were cotransfected with plasmids that encode vesicular stomatitisvirus glycoprotein, NLBH, and shRNAs. Two days after transfection, supernatants that contained viruses were collected and used to infect 293T cells in the presence of polybrene (8 mg/ml). After lentiviral infection of HCT116 or K562 cells, addition of puromycin (1mg/ml) selected for cells that stably expressed shRNAs of each target.

Immunoprecipitation assays

For immunoprecipitation assays, HCT116 and HEK293T cells were lysed in lysis buffer (50 mM Tris-HCl (pH 7.5), 200 mM NaCl, 0.5% NP-40, 1 × protease inhibitor cocktail) and incubated with indicated antibodies overnight at 4°C. Protein A/G agarose beads (Gendepot; P9203) were then added, and the mixture was mixed for 3 h at 4°C. Bound proteins were then analyzed by immunoblot with indicated antibodies.

In vitro acetylation assay

In vitro acetylation assays were performed at 30°C for 3 h in 30 μL volumes containing 50 mM Tris-HCl (pH 8.0), 50% Glycerol, 0.5 mM EDTA, 5 mM dithiothreitol, 100 nCi of [^{14}C]-acetyl coA (Perkin Elmer, NEC313) and GST-UHRF1, GST-UHRF1 #1 (residues 1-100), GST-UHRF1 #2 (90-383), GST-UHRF1 #3 (370-685), GST-UHRF1 #4 (675-793), or GST-UHRF1 (393-610) mutants and 0.5 μg of PCAF. Proteins were separated using 12% sodium dodecyl sulfate-polyacrylamide gel electrophoresis (SDS-PAGE) and analyzed by autoradiography.

Electrophoretic mobility shift assay

The binding of hemi-methylated DNA by recombinant UHRF1 SRA domains using gel mobility shift was completed as previously described with only very minor modification (Zhang et al., 2011). Briefly, recombinant GST–UHRF1 SRA proteins (wild-type and mutants) were expressed and purified from *Escherichia coli* using GST-glutathione beads according to the manufacturer's instruction. To test their hemi-mCpG binding activity, ~2.5 μg recombinant GST–SRA fusion protein was incubated with [^{32}p]-labeled hemi-mCpG probes in the binding buffer (10 mM Tris-Cl (pH 7.5), 50 mM NaCl, 5 mM MgCl2, 1 mM DTT, 0.05% NP-40, 5% glycerol, 50 ng/ μl−1 poly(dI-dC)) at 4°C for 20 min. The reactions were then electrophoresed on a 6% polyacrylamide gel in 0.5x TBE buffer at 200 V for 0.5 h. The results were then visualized by autoradiography. The sequences of the forward and reverse strands of the hemi-mCpG probes are 5′-GGGC**C**GCAGGG −3′, 5′-CCCTGCGGGCCC −3′, in which the positions of the methyl-C are shown in bold.

Liquid chromatography–mass spectrometry

Synthetic peptides (UHRF1 K490) (100 mM) were used as substrates in *in vitro* acetylation assay with PCAF. The reaction was stopped with 10% TCA precipitation for 10 min at 4°C. After removing the precipitates by centrifugation, the supernatants were retrieved and acetylated peptides in the supernatants analyzed by liquid chromatography–mass spectrometry (LC–MS) at the Korea Basic Science Institute. The eluted peptides were separated on a Luna column (C18 PepMap 100, 150x1mm 5 micron) with a linear gradient (A: 5% ACN, 0.1% formic acid; B: 95% ACN, 0.1% formic acid) at a flow rate of 50 mL/min. Typically, 5 mL of sample was injected. Mass spectrometry was performed on a linear ion trap mass spectrometer (LCQ DECA XP, Thermo Finnigan) coupled to a nano-LC system (NANOSPACE SI-2, Shiseido). The MS scan range was 160–2000 m/z.

Chromatin isolation

Chromatin-bound proteins were isolated as previously described with only very minor modification (Méndez and Stillman, 2000). Cells were resuspended (4 × 10^{7}cells/ml) in buffer A (10 mM HEPES (pH 7.9), 10 mM KCl, 1.5 mM $MgCl_2$, 0.34 M sucrose, 10% glycerol, 1 mM DTT, 1 × protease inhibitor cocktail, 0.1 mM phenylmethylsulfonyl fluoride). Triton X-100 (0.1%) was added, and the cells were incubated for 5 min on ice. Nuclei were collected in pellet by low-speed centrifugation (5 min, 1,300 × g, 4°C). Nuclei were washed once in buffer A, and then lysed in buffer B (3 mM EDTA, 0.2 mM EGTA, 1 mM DTT, 1 × protease inhibitor cocktail). Insoluble chromatin was collected by centrifugation (5 min, 1,700 × g, 4°C), washed once in buffer B, and centrifuged again under the same conditions. The final chromatin pellet was resuspended in buffer B and sonicated.

Genome-wide DNA methylation profiling

Genomic DNA was isolated from HCT116 cells UHRF1 knocked down HCT116 cells, recovered with wild-type, acetyl-deficient and acetyl-mimetic UHRF1. In all 600ng of input gDNA was required for the bisulfite conversion. Add conversion reagent and incubate in a thermocycler to denature. CT converted DNA was washing and desulphonating with desulphonation buffer. After desulphonation, the DNA was washing again and eluting with 12ul elution buffer. The whole-genome amplification process requires 250ng of input bisulfite-converted DNA, MA1 and creates a sufficient quantity of DNA (1000X amplification) to be used on a single BeadChip in the infinium methylation assay (Illumina RPM and MSM). After amplification, the product is fragmented using a proprietary reagent (FMS), precipitated with 2-propanol (plus precipitating reagent; PM1), and resuspended in formamide-containing hybridization buffer (RA1). The DNA samples are denatured at 95°C for 20 min, then placed in a humidified container for a minimum of 16 h at 48°C allowing CpG loci to hybridize to the 50-mer capture probes. Following hybridization, the BeadChip/Te-Flow chamber assembly was placed on the temperature-controlled Tecan Flowthrough Chamber Rack, and all subsequent washing, extension, and staining were performed by addition of reagents to the Te-Flow chamber. For the allele specific single-base extension assay, primers were extended with a polymerase and labeled nucleotide mix (TEM), and stained with repeated application of STM (staining reagent) and ATM (anti-staining reagent). After staining was complete, the slides were washed with low salt wash buffer (PB1), immediately coated with XC4, and then imaged on the The iScan System. The iScan System is a two-color (532 nm/658 nm) confocal fluorescent scanner with 0.54 μm pixel resolution. The scanner excites the fluorophors generated during signal amplification/ staining of the

allele-specific (one color) extension products on the BeadChips. The image intensities are extracted using Illumina's GenomeStudio software.

QUANTIFICATION AND STATISTICAL ANALYSIS

Raw data of Methylation EPIC array were extracted as beta values for each CpG for each sample using R watermelon package. Beta values were calculated by subtracting background using negative controls on the array and taking the ratio of the methylated signal intensity against the sum of both methylated and unmethylated signals. A beta value of 1-1.0 was reported significant percent methylation, from 0% to 100%, respectively, for each CpG site (Irizarry et al., 2008). Array CpG probes that have detection p value $\geq$ 0.05 (similar to signal to noise) in over 25% samples were filtered out. (I applied a filtering criterion for data analysis; good signal value was required to obtain a detection p value < 0.05). And then filtered data was background correction & dye bias equalization by R methylumi & lumi package. To reduce Infinium I and Infinium II assay bias, corrected signal value was normalized by BMIQ (Beta Mixture Quantile) method. Differentially expressed methylation list were determined using |delta_mean| $\geq$ 0.2 (the difference of methylation signal, avg beta of Case – avg beta of Control) and p value < 0.05 of independent t test in which the null hypothesis was that no difference exists among 2 groups. All data analysis and visualization of differentially expressed genes was conducted using R 3.3.3 (https://www.r-project.org/).